ChemPubSoc Europe

DOI: 10.1002/cssc.201700492

CHEMSUSCHEM Full Papers

Engineering the Pores of Biomass-Derived Carbon: Insights for Achieving Ultrahigh Stability at High Power in High-Energy Supercapacitors

Ranjith Thangavel[+],[a] Karthikeyan Kaliyappan[+],[b] Hari Vignesh Ramasamy,[a] Xueliang Sun,[b] and Yun-Sung Lee*[a]

Electrochemical supercapacitors with high energy density are promising devices due to their simple construction and long-term cycling performance. The development of a supercapacitor based on electrical double-layer charge storage with high energy density that can preserve its cyclability at higher power presents an ongoing challenge. Herein, we provide insights to achieve a high energy density at high power with an ultrahigh stability in an electrical double-layer capacitor (EDLC) system by using carbon from a biomass precursor (cinnamon sticks) in a sodium ion-based organic electrolyte. Herein, we investigated the dependence of EDLC performance on structural, textural, and functional properties of porous carbon engineered by using various activation agents. The results demonstrate that the performance of EDLCs is not only dependent on their textural properties but also on their structural features and surface functionalities, as is evident from the electrochemical studies. The electrochemical results are highly promising and revealed that the porous carbon with poor textural properties has great potential to deliver high capacitance and outstanding stability over 300 000 cycles compared with porous carbon with good textural properties. A very low capacitance degradation of around 0.066% per 1000 cycles, along with high energy density ($\approx$71 Wh kg^{-1}) and high power density, have been achieved. These results offer a new platform for the application of low-surface-area biomass-derived carbons in the design of highly stable high-energy supercapacitors.

Introduction

In this fast-growing economy, electronic devices from small mobile phones to large electrical vehicles form an integral part of our lives.[1,2] Although energy-storage units, such as lithium-ion, lithium–sulfur, or sodium-ion batteries, can power these devices, current energy-storage units fail to satisfy the need for high power delivered in a very short time.[3,4] Sluggish intercalation and conversion processes make these systems a failure for rapid power delivery.[2,3] The role of supercapacitors, with their ability to deliver high power rapidly, has become more crucial recently.[5,6] Depending on the type of electrodes used, supercapacitors are classified as electric double-layer capacitors (EDLCs), pseudocapacitors, or hybrid capacitors.[3,5] Of these types, EDLCs are the simplest and are constructed by immersing two parallel, symmetrical carbon electrodes in an ion-conductive electrolyte.[7,8] In the mechanism of EDLCs, an electrical potential is applied between the two symmetrical electrodes and ions in the electrolyte are separated and adsorbed over the pore walls to form a double layer of charge.[5] A simple charge-separation phenomenon between the two electrodes is the primary charge-storage technique, and the stored electrical energy is delivered by the reversal of this process over a very short time.[3,4]

Unlike pseudocapacitors and hybrid capacitors, which have low cycle lives due to quick deterioration of the electrode material, EDLCs have an extraordinary cycle life ($>$100 000 cycles) because the mechanism in EDLCs is a purely non-faradic, surface-adsorption phenomenon that occurs only over the electrode surface by the formation of a double layer of charge.[9,10] The development of EDLCs with organic electrolytes has advantages over the use of aqueous media. Due to a larger operating potential window, the possibility of high-energy-density supercapacitors systems is easily achieved.[2,3,5] However, EDLCs deliver unsatisfactory specific energy and cyclability at high power rates due to poor ion-adsorption kinetics at the pores, which must be addressed to make the system more superior.

Carbonaceous electrodes and, in particular, activated carbons (ACs) are the primary choice of electrode material for EDLCs because ACs are highly porous with interconnected pores, have high electrical conductivity, and are inexpensive.[11–13] ACs have a wide range of distributed pores combined with a high pore volume, which provides major sites for the adsorption of ions. The presence of a very high surface area (usually $>$2000 m^2 g^{-1}) in carbon is the primary key to scale up the energy density of EDLCs.[14,15] Additionally, they possess

[a] R. Thangavel,[+] H. V. Ramasamy, Prof. Y.-S. Lee
Faculty of Applied Chemical Engineering
Chonnam National University
Gwang-ju 500-757 (Korea)
Fax: (+82) 625-301-904
E-mail: leeys@chonnam.ac.kr

[b] Dr. K. Kaliyappan,[+] Prof. X. Sun
Department of Mechanical and Materials Engineering
University of Western Ontario
London, N6A 5B9 (Canada)

[+] These authors contributed equally to this work.

Supporting Information for this article can be found under: https://doi.org/10.1002/cssc.201700492.

high chemical and thermal stability that synergistically increase both the power density and cycle life.[16,17]

Although carbon nanotubes (CNTs), carbon aerogels, polymer-derived carbon, and zeolite-derived carbon have emerged as alternatives, they fail at the industrial scale because of both their high cost and their difficult synthesis at large scale. Graphene has also been investigated for EDLC applications.[9,18] Despite impressive electronic conductivity and surface area, the difficulty of preparing single-layer graphene and graphene-layer aggregation reduces its usefulness in EDLCs, which makes ACs the best candidates for EDLCs.[19,20]

Although conventional ACs produced from coal, coke, and tar have high surface areas, they fail at high currents because of considerable ion-diffusional losses that occur due to tortuous pore networks (bottleneck pores).[21–24] Environmental pollution during the activation process is also a cause of global concern.[11,21] Recently, global warming and the scarcity of non-renewable fossil fuels have also triggered the necessity of developing alternative green and renewable resources. Alternative, ecofriendly porous carbons from bioinspired resources may be a good solution to replace conventional ACs, CNTs, graphene, and much more. The vast availability of waste biomass resources is very encouraging for their application in useful energy-storage devices. Every year, millions of tons of biowaste are generated and disposal of this waste is highly challenging, but the conversion of this waste into a useful resource adds value. These bioinspired carbons have properties similar to conventional ACs, and recent research has revealed that they possess better electrochemical properties than conventional ACs.[18,21,22] Biomass-derived porous carbon are a truly green and cheap resource for energy-storage devices. ACs have been successfully synthesized from various natural resources, such as rice husks, peanut shells, corn grains, banana fiber, coconut fiber, pinecone, waste office paper, human hair, wheat straw, and sugarcane waste, and used for various applications.[14–16] The use of biomass-derived carbon in high-energy capacitors can help to develop sustainable energy-storage devices.

However, bioderived ACs still lack a high energy output and good cyclability at high power rates, which limits their ability to satisfy practical needs. Textural factors, such as the specific surface area, pore-size distribution, and pore volume of bioderived ACs, contribute to determining the performance of EDLCs.[17,25,26] Precise control of the textural and structural properties of biomass carbon has not yet been studied for applications in high-energy EDLCs with an organic electrolyte. Although various models, assumptions, and ideas have been proposed to explain the dependence of ionic adsorption on EDLC performance, our understanding of the behavior of ionic adsorption in pores, and the capacitance exhibited, is still at the theoretical stage with modelling and simulation, and must be analyzed for practical purposes by using experimental techniques.[27–29] The correlations of these models are often analyzed for the first few thousand cycles by researchers, but correlations after prolonged cycling or in a high-power environment have not yet been addressed.[30,31] The performance of EDLC systems based on several proposed models and mechanisms requires a much deeper understanding to develop state-of-the-art EDLCs with ultrahigh performance.[27,28,30]

The characteristics of bioderived porous carbons and their performance in EDLCs mainly depend on the type of activation process (physical or chemical) and the activation agent because this controls the pore formation, pore size, pore distribution, and surface functionalities.[11,32,33] During physical activation, precursors are initially carbonized and pores on the carbon surface are formed by CO_2 or steam at high temperature by using an etching process. During chemical activation, the carbon source is impregnated with activation agents, such as alkali metal hydroxides, alkali metal carbonates, H_2SO_4, H_3PO_4, or $ZnCl_2$.[12,14,34] The chemical activation technique is highly preferred to develop porous biomass carbon because of its simple, cheap, and rapid process. The synthesis methodology involves simple precarbonization of the biomass precursor followed by activation of the carbonized product. Chemically activated ACs have uniform pore size distribution along with large number of micropores and, therefore, chemically activated ACs are preferred because they always show superior capacitance performance compared with physically activated carbons.[13,35,36]

Herein, we engineered the pores of ecofriendly porous carbon, derived from cinnamon sticks, by using different activation agents, and evaluated the ionic adsorption behavior for high-energy-density EDLCs. Cinnamon is a member of the species *Cinnamomum* and the inner bark of this tree species is generally referred to as cinnamon sticks. Smaller bark is a general waste byproduct of sawmills and furniture makers. Each activation agent develops different pore structures, pore distributions, and surface functionalities due to different activation mechanisms. This report analyzes the dependence of the structural and textural parameters on the different activation agents, together with the dependence of the electrochemical performance on the structural parameters, which provides deeper insight for the development of high-energy EDLCs. Highly conductive porous carbon with an ultrahigh surface area was prepared from cinnamon sticks by using three different activation agents, namely, KOH, H_3PO_4, and $ZnCl_2$. The as-synthesized carbon was tested for use in EDLCs by using a sodium-based organic electrolyte ($NaClO_4$ in ethylene carbonate/dimethyl carbonate (EC/DMC) to boost the energy density (3 V potential window). Replacement of the lithium-ion electrolyte with a sodium-ion electrolyte is advantageous because the sodium ion has weaker solvation due to its weak Lewis acidity, which thus results in a higher ion-transport number than the lithium analogues and also improved kinetics in the EDLC system.[37]

Herein, we address the parameters that affect the performance of an EDLC at high power and provide a solution to develop highly stable high-energy supercapacitors. Mutual correlations between porosity, pore-size distribution, and surface functionalities synergistically bring about remarkable performance, that is, a very low capacitance degradation of approximately 0.066% per 1000 cycles with 80% stability after 300000 cycles at 3 $kW\,kg^{-1}$. The results obtained were far beyond than those observed for commercially available super-

capacitor systems and should be of great interest to many EDLC manufacturers for the commercialization of this system.

Results and Discussion

The pyrolyzed carbon sample without any activation is denoted as CDC-0 whereas the porous carbons obtained by using KOH, $ZnCl_2$, and H_3PO_4 activation agents are denoted as CDC-1, CDC-2, and CDC-3, respectively. The microstructures of all carbon samples were analyzed by using electron microscopy. The field emission (FE)-SEM images of CDC-0 in Figure S1 in the Supporting Information show a rough surface with no pores and cavities on the surface. The FE-SEM images in Figure 1 show the porous morphology of the particles after activation. All prepared carbons showed an irregular shape, with randomly distributed pores and cavities, regardless of the activation agent. However, the distribution and types of pores on the surfaces were strongly influenced by the activation agent. The pores on the surface of CDC-1 are mostly large, open, and hierarchical. The pores on the CDC-2 surface are not clearly visible and appear highly dense and closed. The surface of CDC-3 shows large cavities in which small pores are embedded. The TEM and high-resolution TEM images presented in Figure 1 reveal that the pores are randomly distributed and are well connected by a nanocarbon framework with no crystalline graphitic impurities. The hierarchal arrangement of pores in CDC-1 can help the pore walls to be fully used for adsorption, whereas the dense and small pores in CDC-2 could impede the fast movement of ions at higher currents. Finally, the cavities in CDC-3 could store a large volume of electrolyte and easily supply it to the embedded pores. The arrangement and structure of the pores in CDC-1 and CDC-3 are more favorable for superior EDLC performance. The wide variation in pore structure over the carbon surfaces is primarily due to the different activation mechanisms that arise from the different activation agents, which have been widely studied.[18,34]

The XRD patterns of the three carbons in Figure 2a show two broad, characteristic peaks for the graphitic plane at around 23 and 44°, which confirmed the amorphous and turbostratic-disordered nature of the carbon.[38,39] The *d*-spacing of the (002) plane for all the carbons was found to be greater than the interlayer spacing of graphite (0.355 nm) owing to a broadening of the planes by activation and carbonization.[39] The highly disordered nature of all the carbons was confirmed by two characteristic peaks in the Raman spectra (Figure 2b): 1) a G band at around 1580 cm^{-1}, assigned to vibration of the

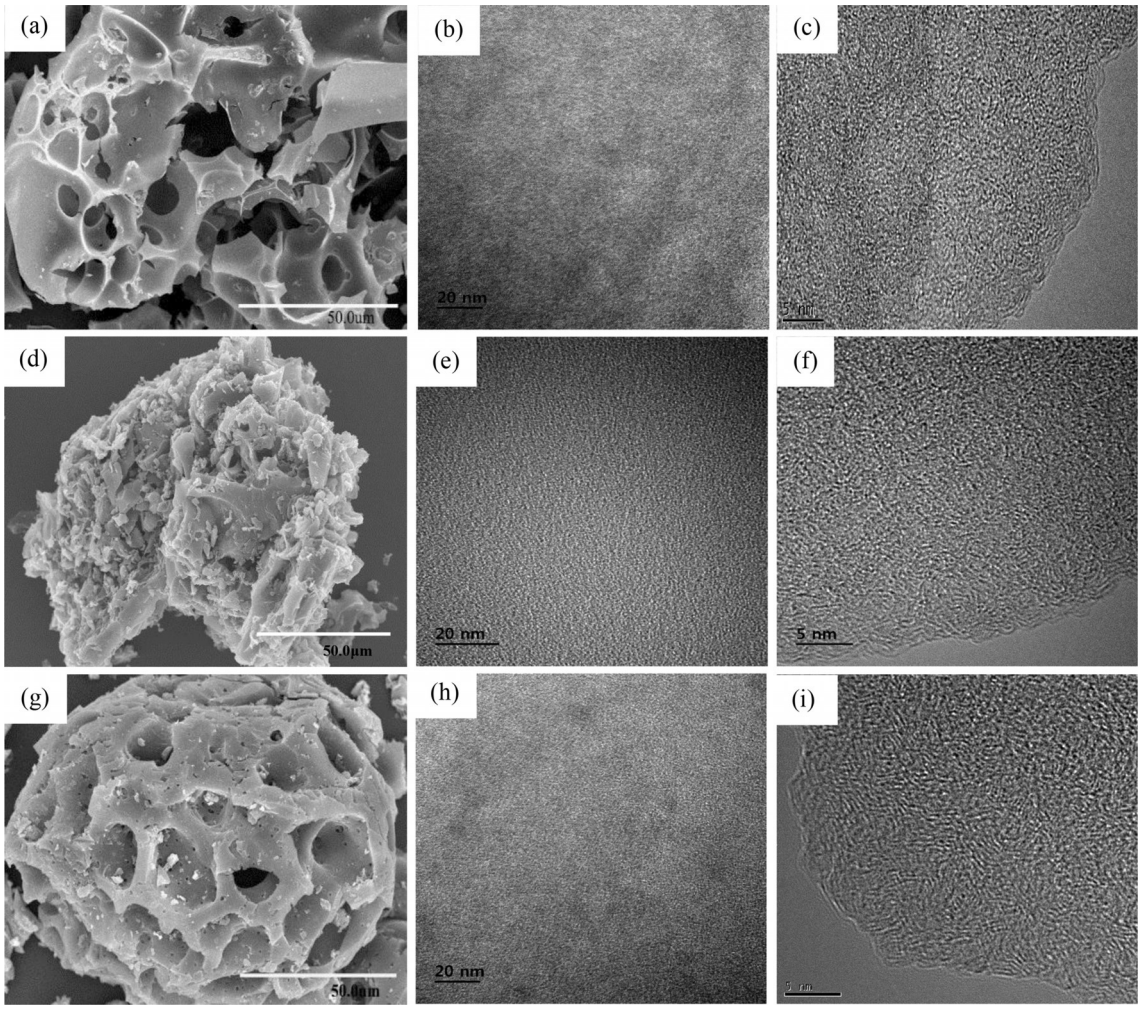

Figure 1. FE-SEM, TEM, and HR-TEM images of a–c) CDC-1, d–f) CDC-2, and g–i) CDC-3. TEM images of d) CDC-1, e) CDC-2, and f) CDC-3.

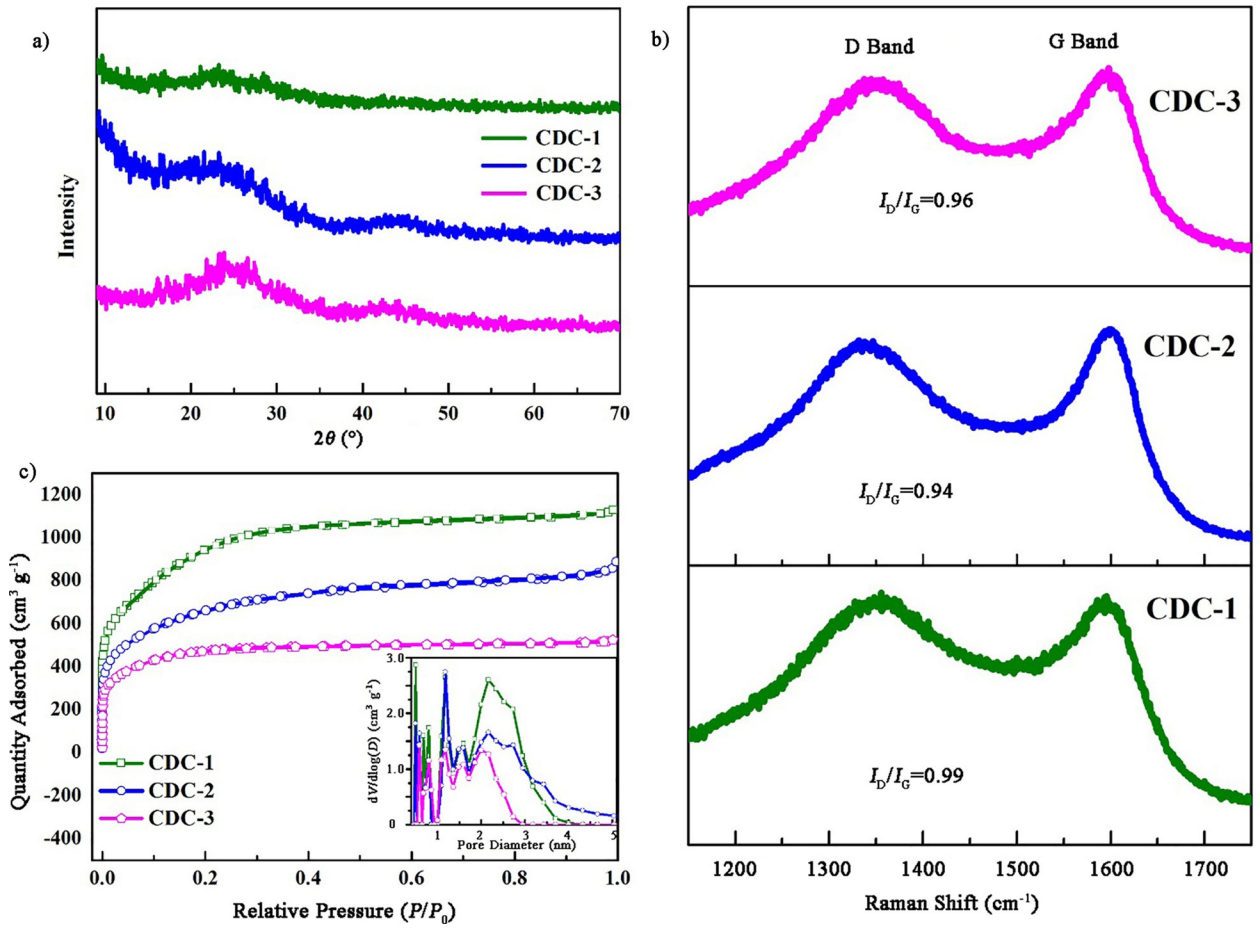

Figure 2. a) XRD pattern of CDCs. b) Raman spectra of CDCs. c) BET isotherms of the CDCs; inset: pore-size distribution of the CDCs calculated by using DFT.

graphitic plane, and 2) a D band at about 1345 cm^{-1}, attributed to a double resonance in disordered carbon.[40] The ratio between the two peaks (I_D/I_G) determines the nature of the carbon and all the carbon samples had a value between 0.99 and 1.04, irrespective of the activation agent, which indicated the amorphous nature of the carbon, with more planar and lattice defects and with high lattice edges.[40,41] Also, the absence of second-order peaks in the wavenumber range of 2400 to 3000 cm^{-1} suggested the absence of a graphitized structure in the porous carbon.[41]

More than the structural and physical properties, the textural properties of carbon can provide insights into its porous nature. Accordingly, nitrogen adsorption/desorption techniques were used to present a clear picture of pore volume, pore size, and pore distribution.[42] The N_2 adsorption/desorption isotherm curve of CDC-0 in Figure S3 revealed type I isotherm behavior and the BET surface area was approximately 520 m^2 g^{-1}. The strong influence of the activation agent on the textural properties of the carbon can be observed from the isotherm curves after the activation process (see Figure 2c). Samples CDC-1 and CDC-2 exhibited a combination of type I and type IV isotherms with a sharp slope at the low partial-pressure region, which indicated the presence of a large number of micropores and a small number of mesopores in the carbon. Sample CDC-3 exhibited a type I isotherm and absorbed all N_2 in the low partial-pressure region, due to the presence of micropores.[43,44] The pore-size distribution curves calculated by using DFT and based on the slit-pore model (see Figure 2c, inset) show the change in pore distribution with different activation agents. Sample CDC-1 has a large quantity of micropores, along with mesopores in the range of 3 to 4 nm. Sample CDC-2 has a combination of micropores and large mesopores distributed over a wide size range, whereas CDC-3 has a much higher concentration of micropores than the other samples, particularly in the range of 0.5 to 0.6 nm, with a narrow pore-size distribution, few mesopores smaller than 3 nm, and almost no pores larger than 3 nm.[45] Micropores greatly aid in double-layer formation, particularly when the pore distribution is very narrow; however, it is believed that a large number of macro- and mesopores can retard the performance of EDLCs at high currents because ions cannot approach them in a very short time to form a double layer.[31] It could be concluded from the adsorption/desorption results that better cycling stability would be expected from an EDLC with CDC-3 electrodes. The various structural and textural properties of CDC-1, CDC-2, and CDC-3 are compared in Table 1.

Table 1. Comparison of textural and structural parameters of the CDCs.

Sample	$d_{(002)}$ [nm]	I_D/I_G	S_{BET} [$m^2\,g^{-1}$]	V_t [$cm^3\,g^{-1}$]	Mean pore diameter [nm]	Pore content [%] micropores	mesopores
CDC-1	0.394	0.99	3405	1.69	1.91	75	25
CDC-2	0.401	0.94	2440	1.32	2.24	69	31
CDC-3	0.381	0.96	1810	0.82	1.84	84	16

[a] BET surface area. [b] V_t = pore volume.

In addition to the textural properties, the surface functionalities and heteroatoms present in the carbon also govern EDLC performance, particularly at higher currents, by improving the wettability of carbon by the electrolyte and reducing the electrode–electrolyte interfacial resistance.[46–48] The X-ray photoelectron spectroscopy (XPS) spectrum in Figure S4 reveals the presence of a C 1s spectrum with a major C—C bond signal at around 284.8 eV, which confirmed the highly carbonaceous nature of all samples.[11,22] Samples CDC-1 and CDC-3 showed a low C/O ratio, which indicated the presence of large number of oxygen-containing functional groups. A high C/O ratio in CDC-2 indicated its highly carbonaceous nature and the presence of a very low quantity of oxygen functional groups. This could unfavorably result in poor surface wetting by the organic electrolyte. The deconvoluted C 1s spectrum shows the presence of various oxygen-containing functional groups, such as phenolic (286 eV), and carboxylic (289 eV) groups. A strong influence of the activation agent on the quantity of functional groups on the carbon surface is clearly seen, and the percentages of various functional groups in the CDC samples are given in Table 2. Sample CDC-3 showed a very high percentage (44 at%) of phenolic (C-OH) functional group than the other samples. In addition, the use of H_3PO_4 as an activation agent incorporated in situ phosphorous heteroatoms into the carbon framework of CDC-3. The high-resolution P 2p spectrum of CDC-3 shows a major peak at around 133 eV, which corresponds to P—C bonds and confirms the successful incorporation of phosphorous atoms into the carbon framework. The percentage of phosphorous was calculated to be 3.04 at%, which is much higher than earlier reports, and this strategy greatly reduces the need for a second treatment for heteroatom doping.[48,49] The presence of P atoms in the carbon framework can increase the active sites for ionic adsorption and also facilitates the adsorption of ions from the electrolyte.[50] A high rate performance can be achieved despite poor textural properties. Moreover, the large quantity of oxygen heteroatoms in CDC-1 and CDC-3 can provide an enormous number of active sites for ionic adsorption, whereas the low percentage of functional groups in CDC-2 reduces the surface wettability by the organic electrolyte and increases the surface–electrolyte interface resistance.[46,51]

Table 2. Comparison of various oxygen containing functional groups contents in the CDCs.

Sample	C/O	Content [at%] graphitic 284.6–285 eV	phenolic 286–286.8 eV	carboxyl ester 288.8–289 eV
CDC-1	5.6	53.01	36.1	10.89
CDC-2	7.3	67.8	22.1	10.1
CDC-3	4.1	51.01	44	4.99

Electrochemical performance

Two carbon electrodes of equal mass were combined to form a symmetrical EDLC and then tested in an organic electrolyte ($NaClO_4$ in EC/DMC) over a potential window of 0 to 3 V. A large potential window was chosen to maximize the energy density of the system. The organic electrolyte is stable without decomposition, even at high potential, and the potential window used was three times larger than that used in aqueous electrolytes and even higher than that used for the expensive ionic liquids used in some EDLCs.[11,19,22]

The electrochemical performance was first explored by using cyclic voltammetry (CV) studies (Figure 3), and all samples showed well-ordered, rectangular-shaped curves that indicated the double-layer storage mechanism of the system.[52,53] No deviation from a rectangular shape nor the presence of any humps due to pseudocapacitance were observed, which suggested that the obtained capacitance was only due to double-layer formation. However, as the scan rate was increased, CDC-1 and CDC-3 retained their rectangular morphology even at 150 $mV\,s^{-1}$, which demonstrated that they can hold a high specific capacitance even at higher currents (Figure S2).[53] However, sample CDC-2 displayed a distorted curve that represented the poor suitability of the material for applications in high-power EDLCs (Figure S2). The poor performance of CDC-2 is mainly due to its poor and limited ionic diffusion and adsorption in the pores at high current, at which ions have little time to be adsorbed over the surface, whereas CDC-1 and CDC-3 showed a high power capability mainly because of the series of hierarchical pore networks that enabled the ions to gain access deep inside the carbon framework.[54,55] The real performance of all samples was analyzed by using a galvanostatic charge/discharge study (Figure 3b–d), which revealed linear and symmetrical triangular charge/discharge curves for all samples, in agreement with the aforementioned CV measurements. This again confirmed that the primary charge storage mechanism is based on electrical double-layer formation.[52–54] At a current density of 0.5 $A\,g^{-1}$, all samples exhibited a specific capacitance greater than 200 $F\,g^{-1}$; this is due to the maximum use of all pores in the carbon at lower current. With increasing current density, samples CDC-1, CDC-2, and CDC-3 exhibited a high specific capacitance of 158, 134, and 151 $F\,g^{-1}$ at 1 $A\,g^{-1}$, respectively (Figure 4a). This impressive result outperforms other reports based on commercial ACs, template-based carbons, and graphene.[15,53,56–58] In contrast, CDC-0 delivered a poor specific capacitance of 33 $F\,g^{-1}$ at 0.5 $A\,g^{-1}$ (Figure S6). The specific capacitance was enhanced by several orders of magnitude after the activation process. However, as the current density was increased further, the porous samples exhibited their own and different specific capacitance values due to

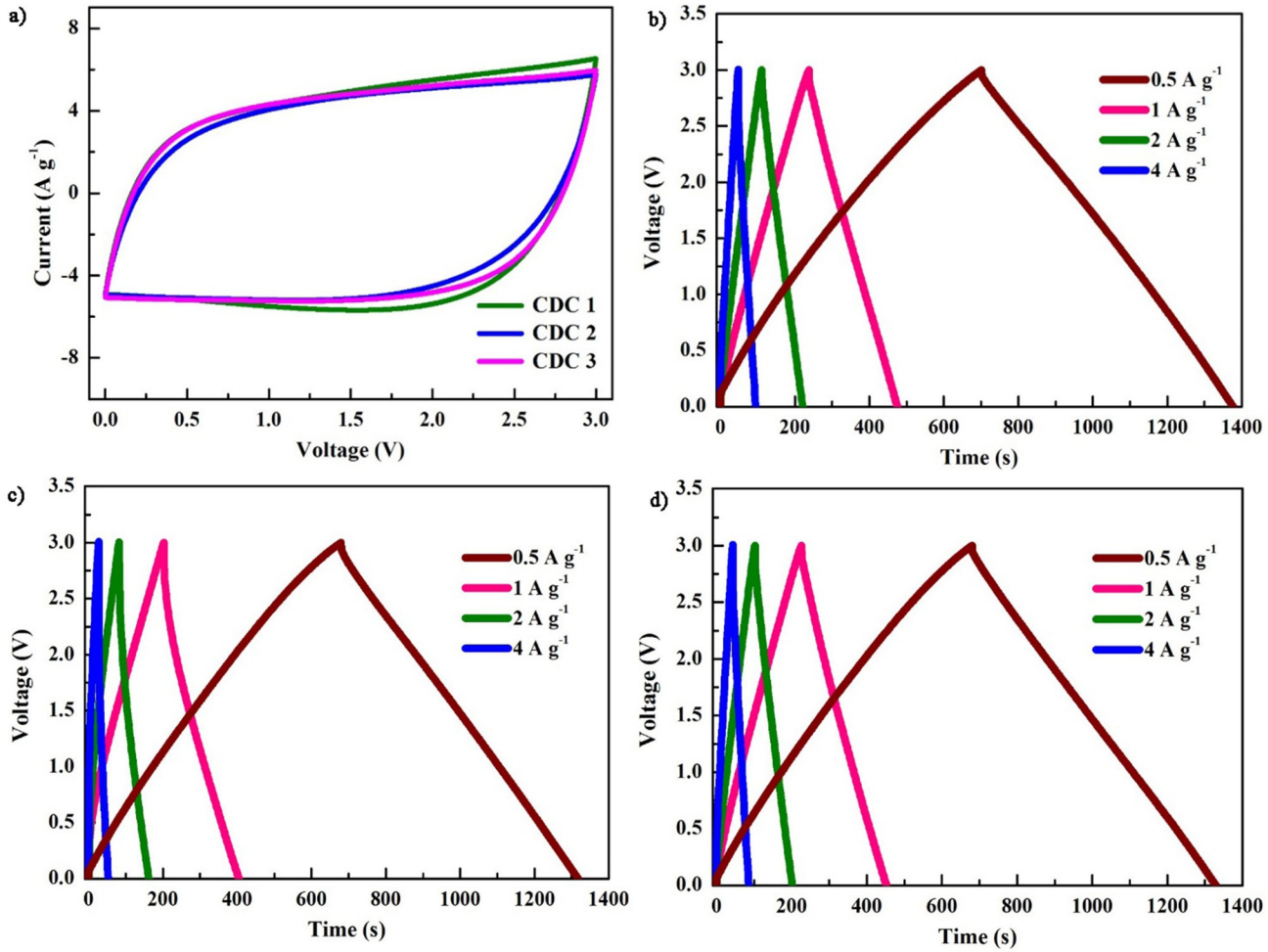

Figure 3. a) CV traces of CDCs at 50 mV s^{-1}. Charge/discharge profiles of b) CDC-1, c) CDC-2, and d) CDC-3 at different current densities.

differences in the interactions between the ions, pores, carbon defects, and functional groups. At 4 Ag^{-1}, samples CDC-1 and CDC-3 delivered specific capacitance values of 126 and 116 F g^{-1}, respectively, whereas CDC-2 delivered a poor specific capacitance of 70 F g^{-1}, which is almost half the value of the others. Even at 8 Ag^{-1}, samples CDC-1 and CDC-3 delivered an impressive specific capacitance values of 96 and 86 F g^{-1}, respectively. Despite a low surface area, CDC-3 exhibited a high capacitance equivalent to high-surface-area CDC-1.

Sample CDC-1 has a large accessible surface area and abundant channels for ionic adsorption and thus delivered a high specific capacitance. However, despite being a carbon with a low surface area and low pore volume, CDC-3 delivered a remarkable specific capacitance, whereas the high surface area and pore volume of CDC-2 delivered a poor specific capacitance (Figure 4b). The traditional understanding that very small pores in carbon with a high surface area cannot be accessed by ions from the electrolyte cannot address this issue because high-surface-area CDC-1 with its large concentration of micropores exhibited high performance.[28,41,59] However, at high currents (8 A g^{-1}), the pores available for adsorption became low for CDC-1 and thus reduced the capacitance. For sample CDC-3, the pores available for adsorption still remained high and delivered a high capacitance equivalent to high-surface-area CDC-1. Samples CDC-1, CDC-2, and CDC-3 have almost the same pore-size distribution in the micropore region, but the presence of long, curved, tortuous, and branched pores in CDC-2 could impede ion movement in the pore entrances under high current conditions, with inadequate time for ions to access the surface of the pores, which would cause severe ohmic drop and diffusion loss.[60,61] With the large mean pore diameters in CDC-1 and CDC-2, the distance between the pore wall and the center of the ion is greatly increased, such that the ions cannot approach the pores in a very short time and, therefore, not all of the pore surface area is used in double-layer formation.[60,62] This was evidenced by the CV curves, which lost their rectangular shape profile and deviated from ideality owing to low pore utilization as the scan rate was increased.[28] The screening effect is also more predominant in large pores due to an increase in the thickness of the double layer formed, which causes CDC-2 to exhibit an inappropriate capacitance. Thus, carbon with a low concentration of micropores and a large mean pore diameter is not an ideal candidate for EDLCs, whereas porous carbon with a small mean pore diameter (< 2 nm) is always preferred.

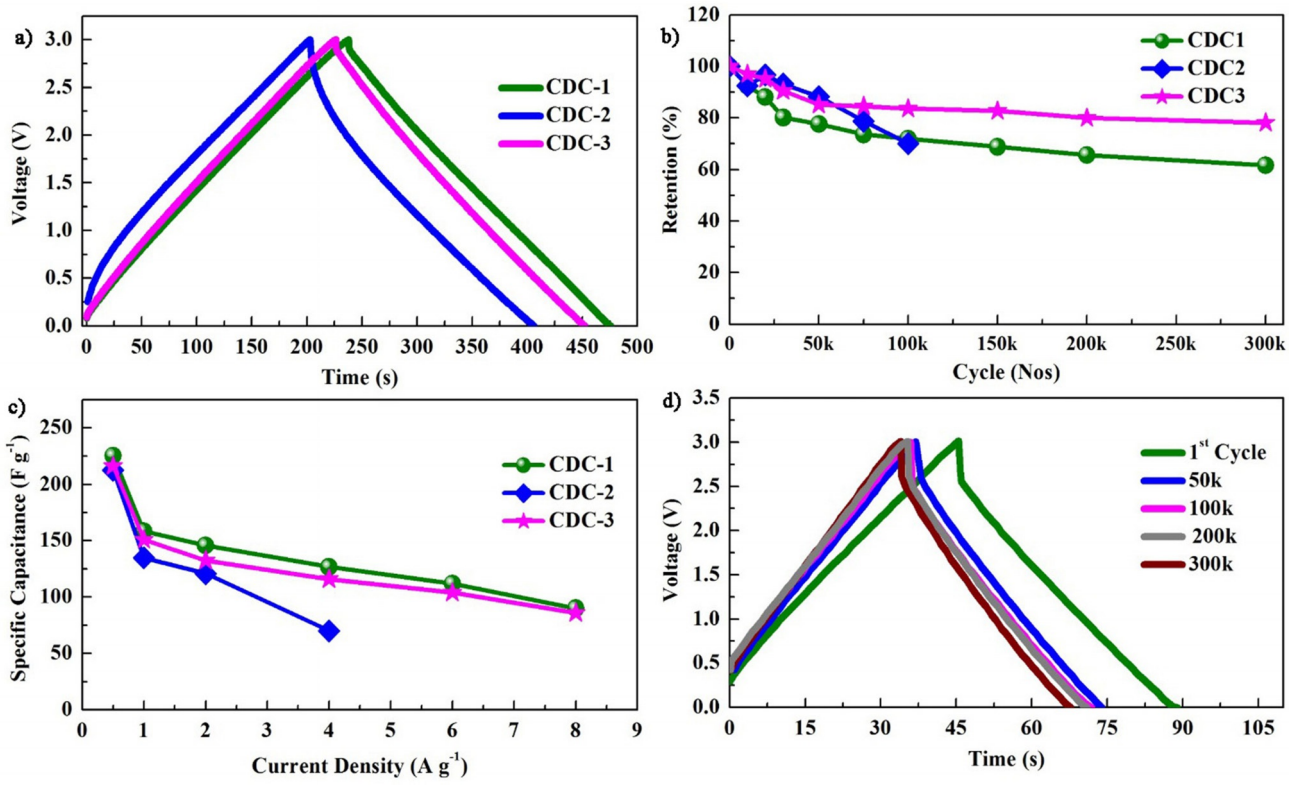

Figure 4. a) Charge/discharge profile for the CDCs at 1 A g^{-1}. b) Rate capability of the CDCs. c) Cyclic stability of the CDCs. d) Charge/discharge curves for CDC-3 at different cycles.

The high specific capacitance of CDC-3 can be ascribed to anomalous capacitance from pores smaller than 1 nm.[27] Sample CDC-3 has a large number of pores in the submicro range (< 0.5 nm), along with a narrower pore distribution and a lower pore volume than the other samples, and solvated Na^+ and ClO_4^- ions sit perfectly in the pores in CDC-3 with no free space around them. Ionic motion is greatly diminished, and the solvation shell of the ions attains a distorted condition in which ions can reach the carbon surface easily and form a double layer, which considerably increases the capacitance.[27,29,30] The ion-storage reservoirs in the sub-micropores provide a very short ion-diffusion path even to deep interior pores.[63] This mechanism is lacking in CDC-2 with its large mean pore diameter, large pore volume, and broader pore-size distribution, which diminishes its performance and particularly its volumetric capacitance. The results indicate that larger pores do not play much of a role in building a double layer; rather, extremely small pores with sizes equivalent to the ionic size of the electrolyte greatly improve the performance. The larger pores can function only as an ion-transport channel or a reservoir for the electrolyte to flow into smaller pores, which facilitates quick ionic transport into the bulk electrode, but they do not contribute to the double layer to a great extent, particularly at higher currents. When these large pores are well interconnected with smaller pores in a hierarchical fashion, they provide easy electron- and ion-transport pathways and, therefore, capacitance can be well maintained at a higher current. A favorable architecture with a narrow pore-size distribution, a large concentration of micropores, and a narrow pore volume in the micropore region, along with a hierarchical macro-meso-micro pore arrangement, synergistically increases the capacitance to a greater level by improving the ion transport kinetics in CDC-3. The P atoms covalently bonded to the carbon framework provide a large number of electrochemically active sites for ionic adsorption, which enhances the capacitance and favors the high-rate performance of CDC-3. Moreover, phosphorous hetero atoms can activate open-edge sites in the carbon to be ion-adsorption sites due to charge delocalization.[64] Furthermore, the capacitance of CDC-3 is enhanced by its large quantity of oxygen-containing functional groups, which provide an enormous number of highly active sites/defects for ionic storage.[65,66]

The long-term cycling stability, a crucial parameter for EDLCs, was tested at 4 A g^{-1}, and the results are shown in Figure 4c. The results demonstrate stability over more than 300 000 cycles, which has never been reported for any system. The typical life expectancy of 100 000 cycles for EDLCs utilizing an aqueous electrolyte has been exceeded several times by this porous carbon/organic system even with a high potential of 3 V. This is the highest stability ever exhibited by an EDLC and outperforms all previously reported EDLCs. A unique feature of the study is the cyclic stability exhibited by CDC-3, which has poorer textural properties than the other samples. Although the specific capacitance of CDC-3 is slightly lower than CDC-1, CDC-3 retained 80% of its initial capacitance and delivered 91 F g^{-1} after 300 000 cycles, whereas CDC-1 delivered

only 77 F g^{-1} with a 61% capacitance retention. The capacitance loss in CDC-3 was calculated to be approximately 0.066% per 1000 cycles, whereas the capacitance losses for CDC-1 and CDC-2 were about 0.126 and 0.206%, respectively (Figure 4d). This is a remarkable performance compared with the average capacitance loss of around 0.5% per 1000 cycles reported for other systems (Table S1).[14,15,18] This extraordinary stability was achieved over a wide working-potential window (0–3 V), whereas many EDLCs require a restricted working window even with ionic liquids (0–2.5 V or 0–2.7 V). This new result demonstrates that the performance of an EDLC should not be estimated only from its textural properties and an initial few thousand cycles. Although CDC-2 delivered poor capacitance, it showed reasonable stability by retaining approximately 80% of its initial capacitance after 75000 cycles, although the test for CDC-2 was terminated at this point because it was not able to deliver sufficient capacitance.

The internal resistance of the cells was analyzed by using electrochemical impedance spectroscopy (EIS), both before and after cycling, and the results are presented in Figure 5a. All cells exhibited a typical semicircle at the medium-to-high frequency region, and an almost vertical line in the low-frequency region. The former is associated with charge transfer resistance while the latter indicates a pure capacitive behavior.[11] Although initially the internal resistances were highly similar, the internal resistances after cycling demonstrated much more variability.[41] A large deviation from ideal behavior was noted for CDC-1 and CDC-2, attributed to high resistance during charge transfer and ionic diffusion of ions into the bulk of the electrode. This is in contrast to the negligible change in resistance exhibited by CDC-3 even after prolonged cycling (300000 cycles), which demonstrated that the adsorption process was still active even inside the deeper pores and that the carbon still retained its intrinsic electronic conductivity after prolonged cycling.[67,68] The sub-micropores in CDC-3 functioned as ion reservoirs and ensured rich ion adsorption sites for a longer time.[69,70] The extraordinary stability behavior of CDC-3 can be mainly attributed to, and is dominated by, the electrochemically stable nature of the oxygen-containing functional groups, aided by the synergistic effect of phosphorous heteroatoms incorporated in the carbon framework.[46] A favorable sub-micro-micro-mesopore distribution coupled by well-connected pores, along with the strong carbon framework in CDC-3, could preserve its structure even under harsh electrochemical testing conditions, which helped to retain its porous nature. The very high C/O ratio in CDC-2, owing to a low percentage of functional groups, was highly disadvantageous because it reduced the adsorption rate of ions, whereas the low C/O ratio and heteroatom in CDC-3 enhanced the adsorption rate and the longevity of the adsorption was well maintained. The poor cyclability of CDC-2 could be attributed to a corrosive effect from the functional groups present.[71] It is known that functional groups can aid in wetting of the carbon and, therefore, the large number of functional groups in the pores of CDC-3 brings in a larger volume of electrolyte compared with CDC-1 and CDC-2, and additionally retains it for a longer time.[58,72,73] The strategy of in situ doping of phosphorous heteroatoms during activation greatly enhanced the stability. Moreover, it plays a crucial role in reducing the surface resistivity by increasing ionic conduction on the surface and by reducing the ion-transport distance, which can be observed from the EIS curves, which aid the efficient performance of the EDLC for a longer time under high-power conditions.[73–75] The various performance features of all porous CDCs are shown in Table 3. This clearly shows that CDC-3 obtained from cinnamon sticks using an H_3PO_4 activating agent would be an excellent candidate for next-generation high-performance EDLCs with ultrahigh stability in a nonaqueous electrolyte.

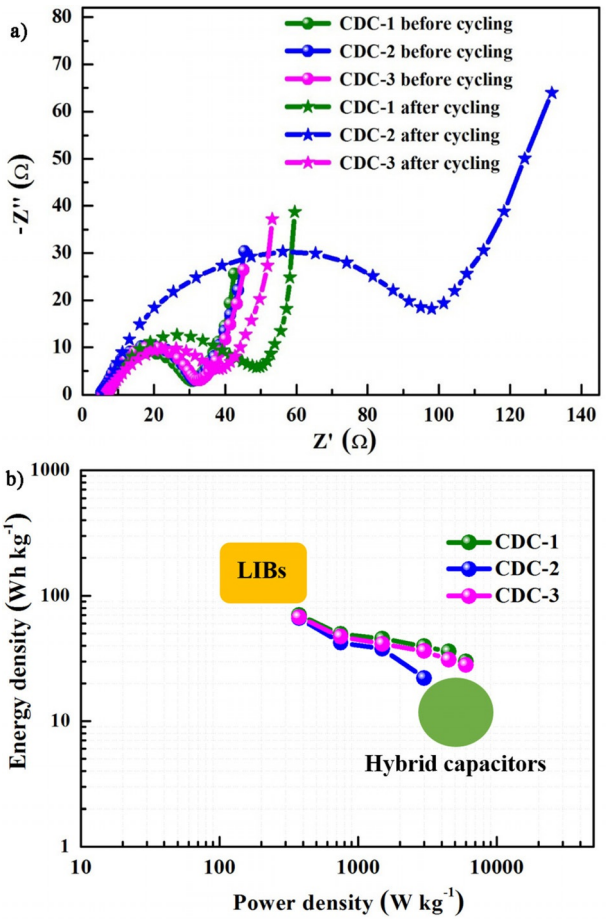

Figure 5. a) Nyquist plots for the CDCs between 200 kHz and 100 mHz before and after cycling. b) Ragone plot for the CDCs.

The Ragone plot in Figure 5b can be used to estimate the practical applicability of the samples. Samples CDC-1, CDC-2, and CDC-3 delivered energy densities of approximately 70, 66, and 68 Wh kg^{-1}, respectively, which are some of the highest values reported for an EDLC based on an inexpensive organic electrolyte. Samples CDC-1 and CDC-3 retained a gravimetric energy density of around 28 and 27 Wh kg^{-1}, respectively, at a specific power density of 6 kW kg^{-1}, which showed that this new EDLC is superior to batteries in terms of power density and far superior to hybrid capacitors in terms of energy retention at high power and cyclability. Although CDC-1 exhibits a slightly higher specific energy density than CDC-3, the higher energy-retention ability of CDC-3 makes it superior to the

Table 3. Performance comparison of various CDCs.

Sample	Specific capacitance [F g^{-1}] (current rate [A g^{-1}])	Energy density [Wh kg^{-1}] (power density [W kg^{-1}])	Power density [kW kg^{-1}] (energy density [Wh kg^{-1}])	Stability [%] (No. cycles)	Energy loss per 1000 cycles [%]	R_{ct} [Ω] before cycling	after cycling
CDC-1	225 (0.5) 90 (8)	70 (375)	6 (28)	62 (300 000)	0.126	23.6	42.3
CDC-2	212 (0.5) 70 (4)	66 (375)	3 (22)	70 (100 000)	0.3	26.5	92.35
CDC-3	217 (0.5) 86 (8)	68 (375)	6 (27)	80 (300 000)	0.0666	26.6	31.47

other samples. With its extraordinary stability, a high specific energy density was retained by CDC-3 even after 300 000 cycles, which far exceeds the performance of every energy-storage system reported to date to the best of our knowledge. Furthermore, low-surface-area CDC-3 can achieve a higher volumetric energy density than high-surface-area CDC-1 and CDC-2. Based on this performance, CDC-3 can satisfy the requirements for hybrid electric vehicle applications and demonstrates to be a high-performance, inexpensive candidate for future energy-storage applications. The performance demonstrated by this new system is compared with other EDLCs, pseudocapacitors, and hybrid capacitor systems in Table S1. Moreover, its stability is superior to all other systems by several orders of magnitude, which thus makes it a suitable candidate for future energy-storage devices. These results are remarkable and outperform all previously reported EDLCs, hybrid capacitors, and even conventional lead–acid batteries, and steadily approaches the performance of present lithium-ion-based systems.[76,77]

Conclusions

The pores of biomass-derived carbon have been explored to develop a new high-energy supercapacitor system that achieved a remarkable stability of over 300 000 cycles with extremely low capacitance degradation (0.066% per 1000 cycles) and a high power density (6 kW kg^{-1}) and a high energy density of about 70 Wh kg^{-1}. The cyclability of the system at high power surpassed all other systems reported to date, with a power density that can compete with modern lithium-based energy-storage systems and hybrid capacitors. Our results pave a new route for the design of carbon materials by overcoming traditional considerations of the dependence of electric double layer capacitor (EDLC) performance on carbon textural properties. Furthermore, the geometry and microstructure of the carbon, along with its surface functionalities, strongly influenced capacitor performance. Our new results emphasize the necessity for long-term stability studies of carbon electrodes to evaluate their real performance.

Experimental Section

Cinnamon sticks purchased from a local food market were used in this study. The cinnamon sticks were thoroughly washed with water to remove surface impurities and dried at 120 °C for 48 h. The clean cinnamon sticks were precarbonized at 300 °C for 2 h in air and then chemically activated with pore-forming agents, namely, KOH, $ZnCl_2$, and H_3PO_4, at 750 °C for 1.5 h under an argon atmosphere. The weight ratio of the carbon precursor to the pore-forming agent was fixed at 1:5 for all samples. The resulting products were washed sequentially with 0.1 M HCl, water, and ethanol to neutralize them to pH 7, then dried under vacuum at 120 °C for 24 h. The pyrolyzed carbon sample without any activation is denoted as CDC-0. The porous carbons obtained by using KOH, $ZnCl_2$, and H_3PO_4 activation agents are denoted as CDC-1, CDC-2, and CDC-3, respectively.

Characterization

Physical characterization

X-ray diffraction (XRD) patterns for the CDCs were recorded by using a Rigaku Rint 1000 diffractometer (Japan) with $Cu_{K\alpha}$ as a radiation source. Raman spectra for the CDCs were obtained by using a Raman dispersive spectrometer (Lab Ram HR 800 Horiba, Japan). The Brunauer–Emmett–Teller (BET) surface areas of the CDCs were calculated from nitrogen adsorption/desorption isotherm measurements, which were performed by using a Micromeritics ASAP 2010 analyzer. The morphological features of the CDCs were recorded by using field-emission scanning electron microscopy (FE-SEM; S4700, Hitachi, Japan) and transmission electron microscopy (TEM; TecnaiF20, Philips, Holland).

Electrochemical characterization

Electrodes were prepared by using Ketjen black (KB) and Teflonized acetylene black (TAB) as the conductive carbon and the binder, respectively. The ratio of active material to KB and TAB was maintained at 80:10:10. The resultant slurry was pasted over a stainless-steel mesh (200 m^2 area) and dried at 160 °C for 4 h before use, and all of the electrochemical measurements were performed in a standard CR2032 coin cell with a mass loading of ≈2.5–3.5 mg cm^{-2}. Two symmetrical AC electrodes were separated using a porous polypropylene (Celgard 3401, USA) separator and filled with $NaClO_4$ in EC/DMC (1:1 *v*/*v*). Cyclic voltammetry (CV) and electrochemical impedance spectroscopy (EIS) studies were carried out by using a Bio-Logic (SP-150, France) electrochemical workstation. Galvanostatic studies were performed between 0–3 V at different current densities by using a Won-A-Tech WBCS 3000 (Korea) cycle tester. The specific capacitance calculation was based on the formula $C_s = 2(I \times t)/(V \times m)$, in which I is the current [A], t is the discharge time [s], V is the operating voltage [V], and m is the mass of CDC in each electrode [g].

Acknowledgements

This work was supported by a National Research Foundation of Korea (NRF) grant funded by the Korea government (Ministry of Science, ICT & Future Planning; no. 2016R1A4A1012224).

Conflict of interest

The authors declare no conflict of interest.

Keywords: biomass · carbon · energy density · mesoporous materials · supercapacitors

[1] S. Chu, A. Majumdar, *Nature* **2012**, *488*, 294.
[2] J. R. Miller, P. Simon, *Science* **2008**, *321*, 651.
[3] P. Simon, Y. Gogotsi, *Nat. Mater.* **2008**, *7*, 845.
[4] Y. Zhai, Y. Dou, D. Zhao, P. F. Fulvio, R. T. Mayes, S. Dai, *Adv. Mater.* **2011**, *23*, 4828.
[5] B. E. Conway, *Electrochemical Supercapacitors: Scientific Fundamentals and Technological Applications*, Springer, New York, **2013**.
[6] Y. Li, Z.-Y. Fu, B.-L. Su, *Adv. Funct. Mater.* **2012**, *22*, 4634.
[7] G. Wang, L. Zhang, J. Zhang, *Chem. Soc. Rev.* **2012**, *41*, 797.
[8] A. Ghosh, Y. H. Lee, *ChemSusChem* **2012**, *5*, 480.
[9] L. L. Zhang, X. S. Zhao, *Chem. Soc. Rev.* **2009**, *38*, 2520.
[10] Y. Zhang, S. Liu, X. Zheng, X. Wang, Y. Xu, H. Tang, F. Kang, Q.-H. Yang, J. Luo, *Adv. Funct. Mater.* **2017**, *27*, 1604687.
[11] K. Karthikeyan, S. Amaresh, S. N. Lee, X. Sun, V. Aravindan, Y.-G. Lee, Y. S. Lee, *ChemSusChem* **2014**, *7*, 1435.
[12] Y. Yang, L. He, C. Tang, P. Hu, X. Hong, M. Yan, Y. Dong, X. Tian, Q. Wei, L. Mai, *Nano Res.* **2016**, *9*, 2510.
[13] L.-Q. Mai, A. Minhas-Khan, X. Tian, K. M. Hercule, Y.-L. Zhao, X. Lin, X. Xu, *Nat. Commun.* **2013**, *4*, 2923.
[14] E. Frackowiak, F. Béguin, *Carbon* **2001**, *39*, 937.
[15] J. Zhang, X. S. Zhao, *ChemSusChem* **2012**, *5*, 818.
[16] M. S. Balathanigaimani, W.-G. Shim, M.-J. Lee, C. Kim, J.-W. Lee, H. Moon, *Electrochem. Commun.* **2008**, *10*, 868.
[17] W. Huang, H. Zhang, Y. Huang, W. Wang, S. Wei, *Carbon* **2011**, *49*, 838.
[18] M. Inagaki, H. Konno, O. Tanaike, *J. Power Sources* **2010**, *195*, 7880.
[19] W. Shi, J. Zhu, D. H. Sim, Y. Y. Tay, Z. Lu, X. Zhang, Y. Sharma, M. Srinivasan, H. Zhang, H. H. Hng, Q. Yan, *J. Mater. Chem.* **2011**, *21*, 3422.
[20] F. Yao, D. T. Pham, Y. H. Lee, *ChemSusChem* **2015**, *8*, 2284.
[21] M. Biswal, A. Banerjee, M. Deo, S. Ogale, *Energy Environ. Sci.* **2013**, *6*, 1249.
[22] J. Ding, H. Wang, Z. Li, K. Cui, D. Karpuzov, X. Tan, A. Kohandehghan, D. Mitlin, *Energy Environ. Sci.* **2015**, *8*, 941.
[23] D. Hulicova-Jurcakova, M. Seredych, G. Q. Lu, T. J. Bandosz, *Adv. Funct. Mater.* **2009**, *19*, 438.
[24] R. Thangavel, B. Moorthy, D. K. Kim, Y.-S. Lee, *Adv. Energy. Mater.* **2017**, 1602654.
[25] K. I. Park, M. Lee, Y. Liu, S. Moon, G. T. Hwang, G. Zhu, J. E. Kim, S. O. Kim, D. K. Kim, Z. L. Wang, K. J. Lee, *Adv. Mater.* **2012**, *24*, 2999.
[26] C. Portet, Z. Yang, Y. Korenblit, Y. Gogotsi, R. Mokaya, G. Yushin, *J. Electrochem. Soc.* **2009**, *156*, A1.
[27] J. Chmiola, G. Yushin, Y. Gogotsi, C. Portet, P. Simon, P. L. Taberna, *Science* **2006**, *313*, 1760.
[28] L. Eliad, G. Salitra, A. Soffer, D. Aurbach, *J. Phys. Chem. B* **2001**, *105*, 6880.
[29] C. Merlet, B. Rotenberg, P. A. Madden, P.-L. Taberna, P. Simon, Y. Gogotsi, M. Salanne, *Nat. Mater.* **2012**, *11*, 306.
[30] H. Ji, X. Zhao, Z. Qiao, J. Jung, Y. Zhu, Y. Lu, L. L. Zhang, A. H. MacDonald, R. S. Ruoff, *Nat. Commun.* **2014**, *5*, 3317.
[31] C. Largeot, C. Portet, J. Chmiola, P.-L. Taberna, Y. Gogotsi, P. Simon, *J. Am. Chem. Soc.* **2008**, *130*, 2730.
[32] D. Hulicova-Jurcakova, A. M. Puziy, O. I. Poddubnaya, F. Suárez-García, J. M. D. Tascón, G. Q. Lu, *J. Am. Chem. Soc.* **2009**, *131*, 5026.
[33] M. Sevilla, R. Mokaya, *Energy Environ. Sci.* **2014**, *7*, 1250.
[34] J. Wang, S. Kaskel, *J. Mater. Chem.* **2012**, *22*, 23710.
[35] L. Zhao, L.-Z. Fan, M.-Q. Zhou, H. Guan, S. Qiao, M. Antonietti, M.-M. Titirici, *Adv. Mater.* **2010**, *22*, 5202.
[36] R. Thangavel, K. Kaliyappan, K. Kang, X. Sun, Y.-S. Lee, *Adv. Energy Mater.* **2016**, *6*, 1502199.
[37] M. Dahbi, N. Yabuuchi, K. Kubota, K. Tokiwa, S. Komaba, *Phys. Chem. Chem. Phys.* **2014**, *16*, 15007.
[38] T.-W. Kim, I.-S. Park, R. Ryoo, *Angew. Chem. Int. Ed.* **2003**, *42*, 4375; *Angew. Chem.* **2003**, *115*, 4511.
[39] W. Zhang, H. Lin, Z. Lin, J. Yin, H. Lu, D. Liu, M. Zhao, *ChemSusChem* **2015**, *8*, 2114.
[40] P. Tan, S. Dimovski, Y. Gogotsi, *Philos. Trans. R. Soc. London Ser. A* **2004**, *362*, 2289.
[41] L. Wei, M. Sevilla, A. B. Fuertes, R. Mokaya, G. Yushin, *Adv. Funct. Mater.* **2012**, *22*, 827.
[42] H. Yang, M. Yoshio, K. Isono, R. Kuramoto, *Electrochem. Solid-State Lett.* **2002**, *5*, A141.
[43] W.-H. Zhang, J.-L. Shi, H.-R. Chen, Z.-L. Hua, D.-S. Yan, *Chem. Mater.* **2001**, *13*, 648.
[44] W.-H. Zhang, J.-L. Shi, L.-Z. Wang, D.-S. Yan, *Chem. Mater.* **2000**, *12*, 1408.
[45] G. Y. Gor, M. Thommes, K. A. Cychosz, A. V. Neimark, *Carbon* **2012**, *50*, 1583.
[46] J. Shen, A. Liu, Y. Tu, G. Foo, C. Yeo, M. B. Chan-Park, R. Jiang, Y. Chen, *Energy Environ. Sci.* **2011**, *4*, 4220.
[47] M.-S. Balogun, W. Qiua, F. Lyu, Y. Luo, H. Meng, J. Li, W. Mai, L. Mai, Y. Tong, *Nano Energy* **2016**, *26*, 446.
[48] Y. J. Kim, C.-M. Yang, K. C. Park, K. Kaneko, Y. A. Kim, M. Noguchi, T. Fujino, S. Oyama, M. Endo, *ChemSusChem* **2012**, *5*, 535.
[49] G. Hasegawa, T. Deguchi, K. Kanamori, Y. Kobayashi, H. Kageyama, T. Abe, K. Nakanishi, *Chem. Mater.* **2015**, *27*, 4703.
[50] Y. Wen, B. Wang, C. Huang, L. Wang, D. Hulicova-Jurcakova, *Chem. Eur. J.* **2015**, *21*, 80.
[51] L.-H. Yao, M.-S. Cao, H.-J. Yang, X.-J. Liu, X.-Y. Fang, J. Yuan, *Comput. Mater. Sci.* **2014**, *85*, 179.
[52] T. Kim, G. Jung, S. Yoo, K. S. Suh, R. S. Ruoff, *ACS Nano* **2013**, *7*, 6899.
[53] T. Y. Kim, H. W. Lee, M. Stoller, D. R. Dreyer, C. W. Bielawski, R. S. Ruoff, K. S. Suh, *ACS Nano* **2011**, *5*, 436.
[54] L. L. Zhang, X. Zhao, M. D. Stoller, Y. Zhu, H. Ji, S. Murali, Y. Wu, S. Perales, B. Clevenger, R. S. Ruoff, *Nano Lett.* **2012**, *12*, 1806.
[55] M. Ghaffari, Y. Zhou, H. Xu, M. Lin, T. Y. Kim, R. S. Ruoff, Q. M. Zhang, *Adv. Mater.* **2013**, *25*, 4879.
[56] X. Zhang, H. Zhang, C. Li, K. Wang, X. Sun, Y. Ma, *RSC Adv.* **2014**, *4*, 45862.
[57] W. Gu, G. Yushin, *WIREs Energy Environ.* **2014**, *3*, 424.
[58] Y. Wang, Z. Shi, Y. Huang, Y. Ma, C. Wang, M. Chen, Y. Chen, *J. Phys. Chem. C* **2009**, *113*, 13103.
[59] D. Lozano-Castelló, D. Cazorla-Amorós, A. Linares-Solano, S. Shiraishi, H. Kurihara, A. Oya, *Carbon* **2003**, *41*, 1765.
[60] L. Eliad, E. Pollak, N. Levy, G. Salitra, A. Soffer, D. Aurbach, *Appl. Phys. A* **2006**, *82*, 607.
[61] O. Barbieri, M. Hahn, A. Herzog, R. Kötz, *Carbon* **2005**, *43*, 1303.
[62] M. Endo, T. Maeda, T. Takeda, Y. J. Kim, K. Koshiba, H. Hara, M. S. Dresselhaus, *J. Electrochem. Soc.* **2001**, *148*, A910.
[63] Y. Li, Z. Li, P. K. Shen, *Adv. Mater.* **2013**, *25*, 2474.
[64] C. H. Choi, S. H. Park, S. I. Woo, *ACS Nano* **2012**, *6*, 7084.
[65] K.-L. Hong, L. Qie, R. Zeng, Z.-Q. Yi, W. Zhang, D. Wang, W. Yin, C. Wu, Q.-J. Fan, W.-X. Zhang, Y.-H. Huang, *J. Mater. Chem. A* **2014**, *2*, 12733.
[66] H. Wang, D. Mitlin, J. Ding, Z. Li, K. Cui, *J. Mater. Chem. A* **2016**, *4*, 5149.
[67] A. Vu, X. Li, J. Phillips, A. Han, W. H. Smyrl, P. Bühlmann, A. Stein, *Chem. Mater.* **2013**, *25*, 4137.
[68] D. S. Su, R. Schlögl, *ChemSusChem* **2010**, *3*, 136.
[69] D. Sheberla, J. C. Bachman, J. S. Elias, C.-J. Sun, Y. Shao-Horn, M. Dinca, *Nat. Mater.* **2016**, *16*, 220.
[70] D. Y. Chung, K. J. Lee, S.-H. Yu, M. Kim, S. Y. Lee, O.-H. Kim, H.-J. Park, Y.-E. Sung, *Adv. Energy Mater.* **2015**, *5*, 1401309.
[71] L. Hao, X. Li, L. Zhi, *Adv. Mater.* **2013**, *25*, 3899.
[72] Z. Lin, Y. Liu, Y. Yao, O. J. Hildreth, Z. Li, K. Moon, C.-p. Wong, *J. Phys. Chem. C* **2011**, *115*, 7120.
[73] E. Frackowiak, *Phys. Chem. Chem. Phys.* **2007**, *9*, 1774.

[74] C. Wang, Z. Guo, W. Shen, Q. Xu, H. Liu, Y. Wang, *Adv. Funct. Mater.* **2014**, *24*, 5511.
[75] A. Castro-Muñiz, F. Suárez-García, A. Martínez-Alonso, J. M. D. Tascón, T. Kyotani, *ChemSusChem* **2013**, *6*, 1406.
[76] H. Kim, M.-Y. Cho, M.-H. Kim, K.-Y. Park, H. Gwon, Y. Lee, K. C. Roh, K. Kang, *Adv. Energy Mater.* **2013**, *3*, 1500.
[77] J. Yan, J. Liu, Z. Fan, T. Wei, L. Zhang, *Carbon* **2012**, *50*, 2179.

Manuscript received: March 22, 2017
Accepted manuscript online: April 28, 2017
Version of record online: June 5, 2017